Marine Chemistry 216 (2019) 103690

Contents lists available at ScienceDirect

Marine Chemistry

journal homepage: www.elsevier.com/locate/marchem

Diurnal to interannual variability of sea surface pCO_2 and its controls in a turbid tidal-driven nearshore system in the vicinity of the East China Sea based on buoy observations

Qian Liu[a,b], Xu Dong[a,c], Jinshun Chen[a], Xianghui Guo[a], Zhirong Zhang[a], Yi Xu[a], Ningli Huang[d], Minhan Dai[a,*]

[a] State Key Laboratory of Marine Environmental Science, Xiamen University, Xiamen, China
[b] Key Laboratory of Marine Chemistry Theory and Technology, Ministry of Education, Ocean University of China, Qingdao, China
[c] Third Institute of Oceanography, Ministry of Natural Resources, Xiamen, China
[d] Shanghai Marine Meteorological Centre, Shanghai, China

A B S T R A C T

We examined the diurnal to seasonal dynamics of the sea surface partial pressure of carbon dioxide (pCO_2) in a subtropical nearshore estuarine system, Hangzhou Bay, adjacent to the Changjiang Estuary in the vicinity of the East China Sea, based on data collected between July 30, 2010 to September 20, 2011 by a surface buoy equipped with an autonomous pCO_2 system along with hydrological and other chemical sensors. The study site (122.37° E, 30.55° N) is influenced by the river plumes of both the Changjiang and Qiantang River and is characterized by strong tidal circulation and highly turbid waters. The amplitude of pCO_2 changes increased from winter to summer over both diurnal and spring-neap tidal cycle timescales. The average surface water pCO_2 was slightly undersaturated with respect to the atmosphere in winter (382 ± 18 μatm), but supersaturated in spring (500 ± 56 μatm) and summer (687 ± 110 μatm). Overall the study site was a source of atmospheric CO_2 with an average sea to air flux of 14 ± 9 mmol C m^{-2} d^{-1} from January to October 2011. We revealed factors controlling the pCO_2 dynamics at different timescales. Over seasonal timescales, temperature and estuarine mixing dominated the seawater pCO_2 variability. Over spring-neap tidal timescales in winter and spring, the major drivers were similarly water mass mixing and temperature. However, in summer, biological activity and air-sea exchange became the two principal factors controlling the variations in surface seawater pCO_2. Our mass balance models further suggested that biological processes impacted surface pCO_2 differently during different tidal phases. Respiration was revealed to promote the increase in pCO_2 during spring tide in August, but in neap tides of the same month biological production was evident and resulted in the drawdown of pCO_2. This is because photosynthesis was generally limited by light in summer at the study site due to high turbidity, except during neap tides when turbidity was dramatically drawn down, triggering high biological productivity. At the diurnal timescale, sea surface pCO_2 was primarily controlled by tidal mixing, except during neap tides in summer when sea surface pCO_2 was greatly influenced by biological metabolism. This study also revealed significant inter-summer differences between 2010 and 2011, showing lower sea surface pCO_2 in August 2010 as compared to August 2011, which was likely due to the enhanced biological uptake as a result of the relatively low turbidity caused by weak tidal currents and enhanced river flow in August 2010. Our study highlights a highly dynamic system primarily driven by tidal mixing, which not only modulates water mass mixing but also affects turbidity, which subsequently controls biological production. These processes led to a synergy of CO_2 dynamics in a tidally driven and highly turbid nearshore system, where high frequency time-series observations are essential to reveal the complex controls of CO_2 dynamics.

1. Introduction

Despite their small surface area, nearshore coastal waters and estuarine systems may exhibit the largest dynamics and heterogeneities in the marine realm in terms of both biogeochemical fluxes and their controls, representing a most difficult component of the coastal carbon cycle (Dai et al., 2009; Bauer et al., 2013; Chen et al., 2013; Bakker et al., 2016; Bourgeois et al., 2016). As a consequence, there are much less publicly available pCO_2 observations in the coastal and estuarine systems compared to open ocean (Bakker et al., 2016). Coastal and estuarine systems are subject to abundant material inputs from land, thus showing greater temporal variations in pCO_2 on both intra-seasonal (short-term) and seasonal scales (Borges and Frankignoulle, 1999; Dai et al., 2009; Bauer et al., 2013; Laruelle et al., 2017). For example, Guo et al. (2009) observed a high seasonal variation of pCO_2, up to ~1000 μatm, in the highly urbanized upper estuary of the Pearl River. Although some studies have focused on the temporal variability of pCO_2 in nearshore waters, these prior studies are mostly based on observations that have a high spatial resolution but occur over short timescales or long-term timescales with a low frequency, which makes it difficult to resolve the full spectrum of CO_2 dynamics across finer timescales and its fluxes at regional or global scales (Borges and Frankignoulle, 1999;

* Corresponding author.
E-mail address: mdai@xmu.edu.cn (M. Dai).

https://doi.org/10.1016/j.marchem.2019.103690
Received 29 December 2018; Received in revised form 26 July 2019; Accepted 28 July 2019
Available online 29 July 2019

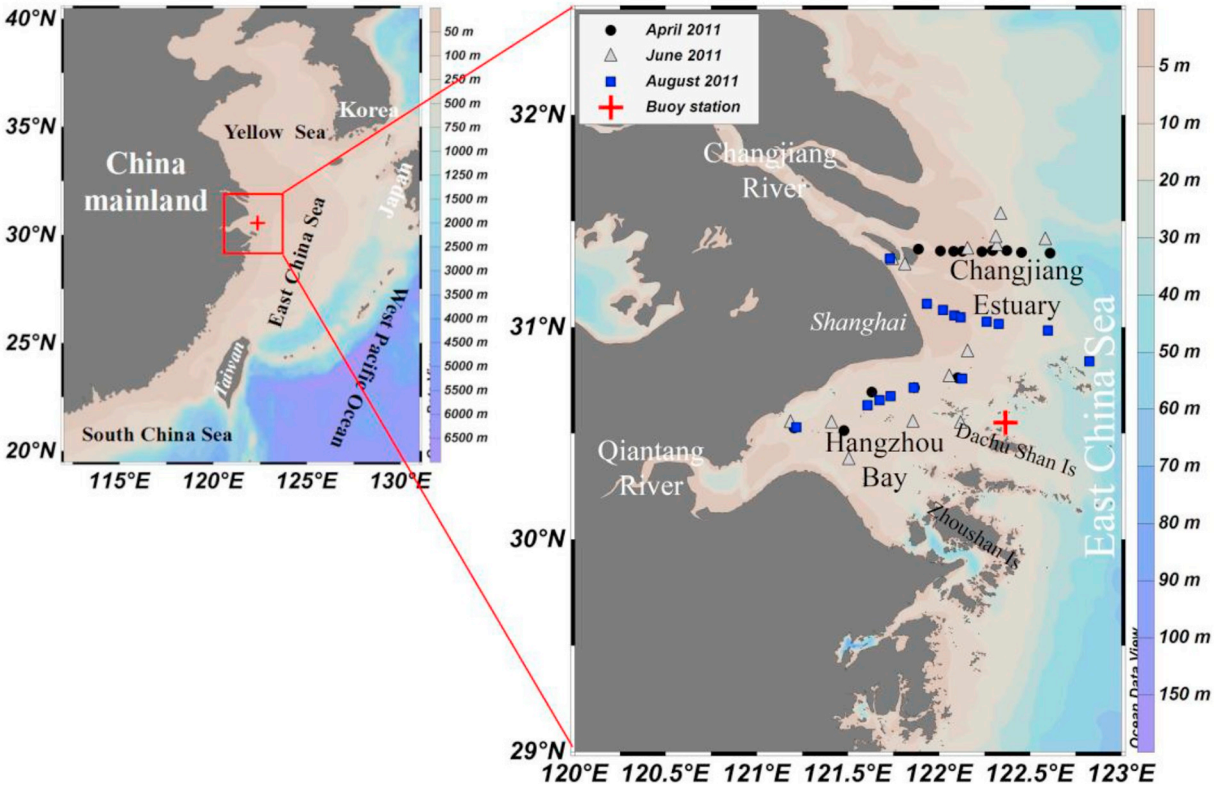

Fig. 1. Map of the East China Sea showing the location of the buoy deployed from August 2010 to September 2011. Also shown are the stations in the Changjiang Estuary, Hangzhou Bay, and inner shelf of the East China Sea sampled during three cruises in April, June, and August 2011. The buoy site was also sampled (the symbols are overlapped). The figure was made with the software of Ocean Data View (Schlitzer, 2013).

Yates et al., 2007; Dai et al., 2009; Schiettecatte et al., 2007).

Mooring platform observations bring the possibility of high frequency pCO_2 measurements over a range of timescales (Lefèvre et al., 2008; Nemoto et al., 2009; Turk et al., 2010; Xue et al., 2016; Reimer et al., 2017; Li et al., 2018), providing important insights about CO_2 dynamics that are otherwise difficult to capture. For example, over a one-year period, surface seawater pCO_2 observations via a moored autonomous pCO_2 system off the coast of Georgia revealed an abrupt drawdown of pCO_2 that was not captured by prior ship-based studies (Xue et al., 2016). Along the Georgia coast, temperature is the main driver for the annual cycle of pCO_2, although riverine inputs through biological respiration and production also significantly contribute to the variation of seawater pCO_2 (Xue et al., 2016). In addition, a seven year time-series study in the Bay of Brest, deployed by a CARIOCA sensor on an automatic moored system, have shown that biological processes play a dominant role in the diurnal, seasonal, and intra-annual variability of pCO_2 (Bozec et al., 2011). These examples clearly demonstrate that the control mechanisms of pCO_2 in the nearshore waters of different regions under different environmental settings may be highly variable.

Numerous studies have indicated that tidal forcing plays an important role in the biogeochemistry of carbon and other biogenic elements in estuarine systems. For example, tidal height and pCO_2 inversely correlated in estuaries along the Taiwan Strait, suggesting tidal mixing was the dominant process controlling variations in surface seawater pCO_2 (Dai et al., 2009). Tidal forcing was observed to significantly affect organic matter exchange between dissolved and particulate pools in tidal estuaries along the Atlantic coast of Europe during both semidiurnal and spring-neap tidal cycles (Middelburg and Herman, 2007). Consistently, the nutrient concentrations in a small California estuary were also predominantly controlled by tidal mixing (Caffrey et al., 2007).

Hangzhou Bay, a subtropical tidal estuary, is located on the inner shelf of the East China Sea (ECS), and influenced by the river plumes from both the Qiantang River and Changjiang (or Yangtze River). The Qiangtang River and Hangzhou Bay are famous for their macrotidal ranges of up to 8 m during spring tide (Wang, 1990). Due to high turbidity, phytoplankton growth in the system is often limited by light penetration, which can change however based on the extent of seawater intrusion into the estuary (Zhou et al., 2012). Limited studies (Gao et al., 2008; Zhai and Dai, 2009) indicate that this area generally behaves as a source of atmospheric CO_2. However, short (diurnal) and long-term (seasonal and inter-annual) monitoring of seawater pCO_2 in this area are scant (Yu et al., 2013; Tseng et al., 2014; Guo et al., 2015). However, the mechanisms controlling surface seawater pCO_2 across different timescales have not been thoroughly examined, and an assessment of the response of pCO_2 to frequently occurring eutrophication events is still lacking.

In this study, we present a large, high frequency data set of pCO_2 and air-sea CO_2 fluxes collected during August 2010–September 2011 based on an autonomous buoy system deployed at the mouth of Hangzhou Bay. We examined the main controls of pCO_2 dynamics over seasonal and neap-spring tidal cycles as well as diurnal timescales. Moreover, we constructed mass balance models to quantify the relative importance of various controlling factors during the spring-tide of summer and in an algal bloom event, which frequently occurs during the summer neap tide. Lastly, we compared monthly pCO_2 in August 2010 with August 2011 and revealed the possible mechanism modulating the inter-summer changes.

2. Material and methods

2.1. Study site

Our study site (122.37° E, 30.55° N) is located at the mouth of Hangzhou Bay and has an average water depth of 30 m. It faces the

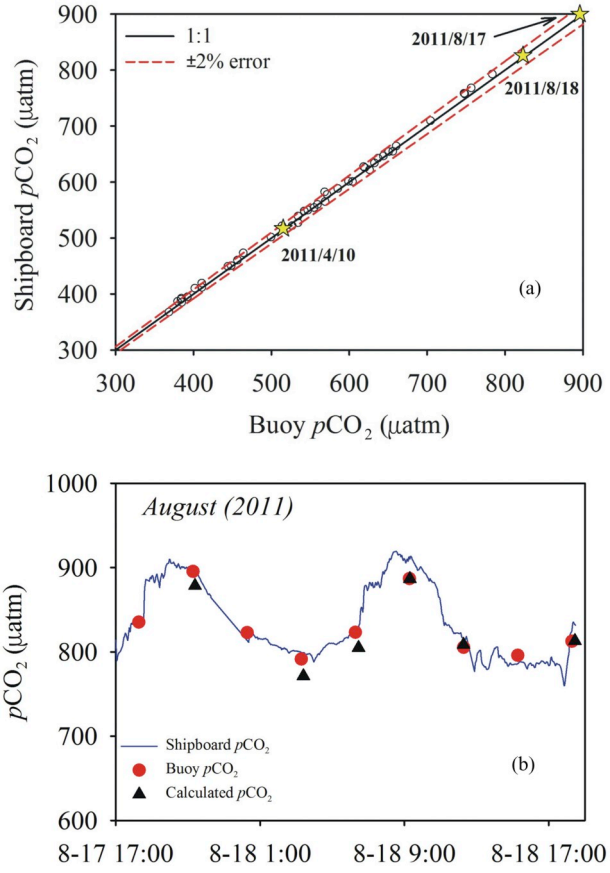

Fig. 2. Underway pCO_2 measurements versus buoy pCO_2 observations deployed in western Xiamen Bay from July 7 to July 15, 2010 (black circles, a) and near the buoy site (~0.5 km away) conducted on April 10, August 17 and 18, 2011 (yellow stars, a). Comparison of buoy surface seawater pCO_2 observations and shipboard time-series measurements of pCO_2 as well as calculated pCO_2 from DIC and TA measured near the buoy site (~0.5 km away) from 17:00 August 17 to 17:00 August 18, 2011 (b). (For interpretation of the references to colour in this figure legend, the reader is referred to the web version of this article.)

Changjiang Estuary to the north, Hangzhou Bay to the west, and the Zhoushan Islands to the south (Fig. 1). The area is characterized by a strong influence of freshwater inputs from both the Changjiang and Qiantang Rivers, and exhibits estuarine mixing with a salinity range of 20 − 30 (Gao et al., 2011). The Changjiang River is the fourth largest river in the world, with an average freshwater discharge of $\sim 944 \times 10^9\ m^3\ yr^{-1}$ (Dai and Trenberth, 2002). Changjiang River fluxes are greater in summer than in winter, and the structure of the Changjiang plume is seasonally variable. In winter the plume flows southward, confined in a narrow band along the coast. In summer, the main pathway of the plume turns to the northeast, with an extension in a band to the south along the coast (Mao et al., 1963; Beardsley et al., 1985). In addition, because of higher discharge in summer, the Changjiang plume obtains ample kinetic energy to run offshore towards the southeast for a distance and then rotates at ~122°30′E to the northeast (Wu et al., 2011). Consequently, the buoy site is affected by the Changjiang plume throughout the year. Moreover, the Qiantang River could also reach the buoy site after passing through Hangzhou Bay, although the mean Qiantang River discharge is only ~4% of the Changjiang River (Ni et al., 2003), particularly in summer when most of the Changjiang plume tends to turn northeast after leaving the Changjiang Estuary. Hangzhou Bay and its adjacent area is a highly turbid system; the average suspended particulate matter (TSM) concentrations reach up to $1.56\ kg\ m^{-3}$ (Chen et al., 2006a,b; Xie et al., 2009). TSM concentrations have distinct seasonal and spring-neap tidal variations, e.g. lower TSM concentrations are generally observed in summer and during the neap tide compared with winter and the spring tide (Chen et al., 2006a,b). This study area featured strong semi-diurnal tidal cycles with a tidal range of 3–4 m (Xie et al., 2009). The velocities of tidal currents during flood and ebb reach ~80 and ~90 cm s^{-1} respectively and the residual surface current exceeds 20 cm s^{-1} (Hu et al., 2009). Therefore, under the impact of strong tides and freshwater from rivers, the biogeochemical processes and carbon cycle at this buoy site might be controlled by tidal mixing. Despite the high turbidity, the mouth of Hangzhou Bay and its adjacent area are frequently reported as sites of red tide/algal blooms in the spring and summer (Zhao et al., 2004; Wang and Wu, 2009).

2.2. Time series observations

Data presented in this study were obtained from July 30 to October 20, 2010, and from January 17 to September 20, 2011, by a 10-m-diameter moored buoy. High frequency measurements performed at 3-h intervals of sea surface pCO_2, atmospheric pCO_2 and other related parameters such as sea surface temperature and salinity (SST and SSS), dissolved oxygen (DO), 10-m-wind speed, wind direction, and turbidity were collected during the deployments. An autonomous CO_2 measurement system, Battelle-CO_2 (© Battelle Memorial Institute), was mounted on the buoy. This Moored Autonomous pCO_2 (MAPCO2) system combined an "h" shaped bubble air-sea equilibrator with a non-dispersive infrared analyzer Li-820 (LI-COR® Inc.). The Li-820 detector performs two-point calibrations automatically with a zero-CO_2 reference before each sampling interval and CO_2 standard gases (501.07 ppm in 2010 and 500.94 ppm in 2011) traceable to World Meteorological Organization (WMO) references (Sutton et al., 2014). Aqueous pCO_2 was estimated as a function of the mole fraction of CO_2 (xCO_2) in dry air, barometric pressure, and saturated water vapor pressure from Weiss and Price (1980), as well as temperature in the equilibrator headspace and of surface seawater. Detailed calculations and measurement principles are presented in Sutton et al. (2014).

2.3. Data quality assessment by shipboard measurements

To assess the data quality of the MAPCO2 system, we compared the buoy data with our homemade underway CO_2 system (1% accuracy, Zhai et al., 2005a,b) during a time-series investigation in western Xiamen Bay (24.5390°N, 118.0632°E, from July 7 to July 15, 2010) before the system was mounted on the buoy. A point to point comparison (circles in Fig. 2a) between the two systems shows almost identical results within ± 2% error. In addition, during the deployment of the buoy, we carried out 3 cruise surveys in April, June, and August 2011 in the vicinity of the buoy site (0.3–0.7 km) to verify the buoy data. For the cruises in April and August, a submersible pump was mounted on the ship at a depth of 0.5–2 m below the sea surface, which was generally consistent with the sampling layer (~0.5 m) by the MAPCO2 system. The underway pumping system continuously measured CO_2 at one-minute intervals. Meanwhile, sea surface temperature and salinity were measured by a YSI® 6600 (YSI® Inc.) at the same interval. Unfortunately, we did not measure sea surface pCO_2 during the survey in June. In addition, discrete samples for dissolved inorganic carbon (DIC), total alkalinity (TA), pH (NBS buffers, 25 °C), and DO were also collected from the side vent of the pumping system in April and August, but from Niskin bottles in June. All samples except TA were free of bubbles. DIC and TA were preserved with saturated $HgCl_2$ and analyzed within two weeks after sampling. The analytical methods for DIC and TA have been described in Cai et al. (2004) and each has a precision of < ± 2 µmol kg^{-1}. The pH at 25 °C was measured on-site with a Corning 350 pH/ion analyzer and a Ross combination electrode (Orions) calibrated against three NIST pH buffers (NBS buffers) at 25 °C. The precision of pH measurements was ± 0.005 units. DO was measured onboard by the classic Winkler titration method at a precision

of ± 1.25 μmol kg^{-1} (0.3%). pCO_2 calculated by DIC and TA (partly by TA and pH) with the CO2SYS program (Pierrot et al., 2009) was used to further validate the observed pCO_2 values and fill up the pCO_2 data gap in June. The dissociation constants of carbonic acid (K_1 and K_2) are from Millero et al. (2006). The value of KSO_4^- is from Dickson (1990). The concentrations of phosphate and silicate used in the CO2SYS program are 1.31 ± 0.12 and 45.0 ± 5.9 μmol kg^{-1} (n = 6), respectively. The comparison between buoy and shipboard system is still within ± 2% error (Fig. 2a). In addition, hourly time-series observations of pCO_2 and other related parameters were carried out onboard from 17:00 Beijing Time, 17 August 2011 to 17:00 Beijing Time, 18 August 2011 in proximity to the buoy (~0.5 km) (Fig. 2b). The relative standard deviations among buoy pCO_2, shipboard pCO_2, and calculated pCO_2 ranged from 0.6% to 1.8% (average 1.3%), which further demonstrated the good quality of pCO_2 data obtained from the MAPCO2 system. The average difference between buoy DO (AADERAA® DO) and Winkler DO (figure not shown) measurements was 4%, which agrees with the accuracy of < 5% given by AADERAA®. Therefore, we have built a reliable in situ pCO_2 observation system on a moored buoy with a Battelle-CO_2 system in an estuary of the ECS. These pCO_2 data will be submitted to SOCAT database (The Surface Ocean CO_2 Atlas, https://www.socat.info/).

2.4. Computational methods

2.4.1. Temperature effect on the variation of pCO_2

To remove the temperature effect, aqueous pCO_2 was normalized to mean sea surface temperature ($\overline{SST}$) following Takahashi et al. (1993, 2002):

$$pCO_{2\_nontherm} = pCO_2 \times e^{0.0423\times(\overline{SST}-SST)} \quad (1)$$

where $pCO_{2\_nontherm}$ is the observed pCO_2 after temperature normalization, representing pCO_2 without a temperature effect. SST is the in situ sea surface temperature and $\overline{SST}$ represents the mean value during the target period.

The thermal forcing on aqueous pCO_2 can be estimated as in Dai et al. (2009),

$$pCO_{2\_therm} = pCO_2 - pCO_{2\_nontherm} = pCO_2 - pCO_2 \times e^{0.0423\times(\overline{SST}-SST)} \quad (2)$$

where pCO_{2_therm} represents aqueous pCO_2 values under the influence of temperature.

2.4.2. Air-sea CO_2 exchange flux

The air-sea CO_2 flux (F) was calculated as

$$F = k \times \alpha \times \Delta pCO_2 = k \times \alpha \times (pCO_{2\,seawater} - pCO_{2\,air}) \quad (3)$$

where k is the CO_2 transfer velocity, α is CO_2 solubility (Weiss, 1974), and ΔpCO_2 is the partial pressure difference of CO_2 between surface seawater and the atmosphere. A positive flux value represents a net CO_2 exchange from the water body to the air. CO_2 transfer velocity as a function of wind speed is determined from Sweeney et al. (2007) as follows,

$$k = f \times u_{10}^2 \times (660/Sc)^{0.5} \quad (4)$$

where, f = 0.27, and u_{10} is the wind speed at 10 m above the sea surface. Sc is the Schmidt number as a function of temperature (Wanninkhof, 1992).

2.4.3. Quantification of factors influencing the surface water pCO_2

We constructed a one-dimensional budget model to evaluate various pCO_2 controlling factors and their uncertainties according to Xue et al. (2016), with the details presented in Appendix S1 and S2.

2.4.4. Biology effect on the variation of pCO_2

The main biological processes consuming and generating CO_2 were illustrated as follows,

$$106CO_2 + 16HNO_3 + H_3PO_4 + 122H_2O \overset{\text{photosynthesis/respiration}}{\leftrightarrow} (CH_2O)_{106}(NO_3)_{16}H_3PO_4 + 138O_2 \quad (5)$$

According to Eq. (5), we calculated the change of DIC (δDIC) due to biological effects and the change of pCO_2 (δpCO_2) was estimated by the Revelle Factor (β) (Revelle and Suess, 1957) as,

$$\beta = (\delta pCO_2/pCO_2)/(\delta DIC/DIC) \quad (6)$$

$$\delta pCO_2 = \beta \times \delta DIC/\overline{DIC} \times \overline{pCO_2} \quad (7)$$

where $\overline{DIC}$ and $\overline{pCO_2}$ represent the average values of each parameter. In this study, β, which is the buffer (Revelle) factor, is ~15.3, calculated using the CO2SYS program from TA and DIC sampled at the buoy site in August (Pierrot et al., 2009). $\overline{DIC}$ was set to 2000 μmol kg^{-1}; a reasonable range in its values would have a minor influence on pCO_2 fluctuations.

3. Results

3.1. Data overview

Shown in Fig. 3 is the time-series data of air temperature, SST, SSS, atmospheric pCO_2, sea surface pCO_2, $pCO_{2\_nontherm}$ (normalized to 19.1 °C), wind speed at height of 10 m above sea surface, and DO saturation via the moored buoy from July 30–October 20, 2010, and January 17–September 20, 2011. Data are not available from October 21, 2010 to January 16, 2011 due to maintenance of the buoy. This unique dataset thus covers two summers, part of fall, one winter and one spring season and allows us to examine timescale variability and its controls. It should be noted that the turbidity data are available and reliable solely in summer (from July to September 2011), and the details are presented in Section 4.3.

SST gradually increased from January (4–5 °C) to August (25–30 °C, Fig. 3b), consistent with the trend in air temperature (Fig. 3a), suggesting that SST was mainly controlled by seasonal warming. Based on these temperature variations, time-series data in this study were divided into three stages/seasons: a low temperature period/winter (January and February), a period of rising temperatures in spring (March to June), and a high temperature period in summer (July to September).

SSS generally had a negative relationship with river discharge. Low SSS corresponded to increased river discharge in summer, suggesting a strong terrestrial influence during this season. However, the variation of mean SSS was not perfectly consistent with river discharge: e.g. from January to May SSS increased gradually from a monthly average of 25.4 to 27.9 (Fig. 3c), despite the Changjiang discharge being constant (~15,000 m^3 s^{-1}) during these periods (Fig. 3d). Additionally, the lowest SSS existed in September, but the highest river flows occurred in June and July (Fig. 3c and d). This discrepancy indicated that the river plume did not fully reach the location of the study site during all seasons. In other words, SSS at the buoy was not solely related to riverine discharge, but also likely affected by large seasonal variations in river plume paths as described in Section 2.1. The monthly discharge of the Changjiang was 14–83 fold greater than the Qiantang River in 2011 (Fig. 3d).

Over the entire study period, sea surface pCO_2 ranged from 170 to 940 μatm, generally arose from winter, spring, to summer (Fig. 3e). The surface water pCO_2 exhibited remarkably large variability with largest amplitudes in summer when it also occurred the maximum and minimum values (Fig. 3e). Atmospheric pCO_2 showed relatively stable

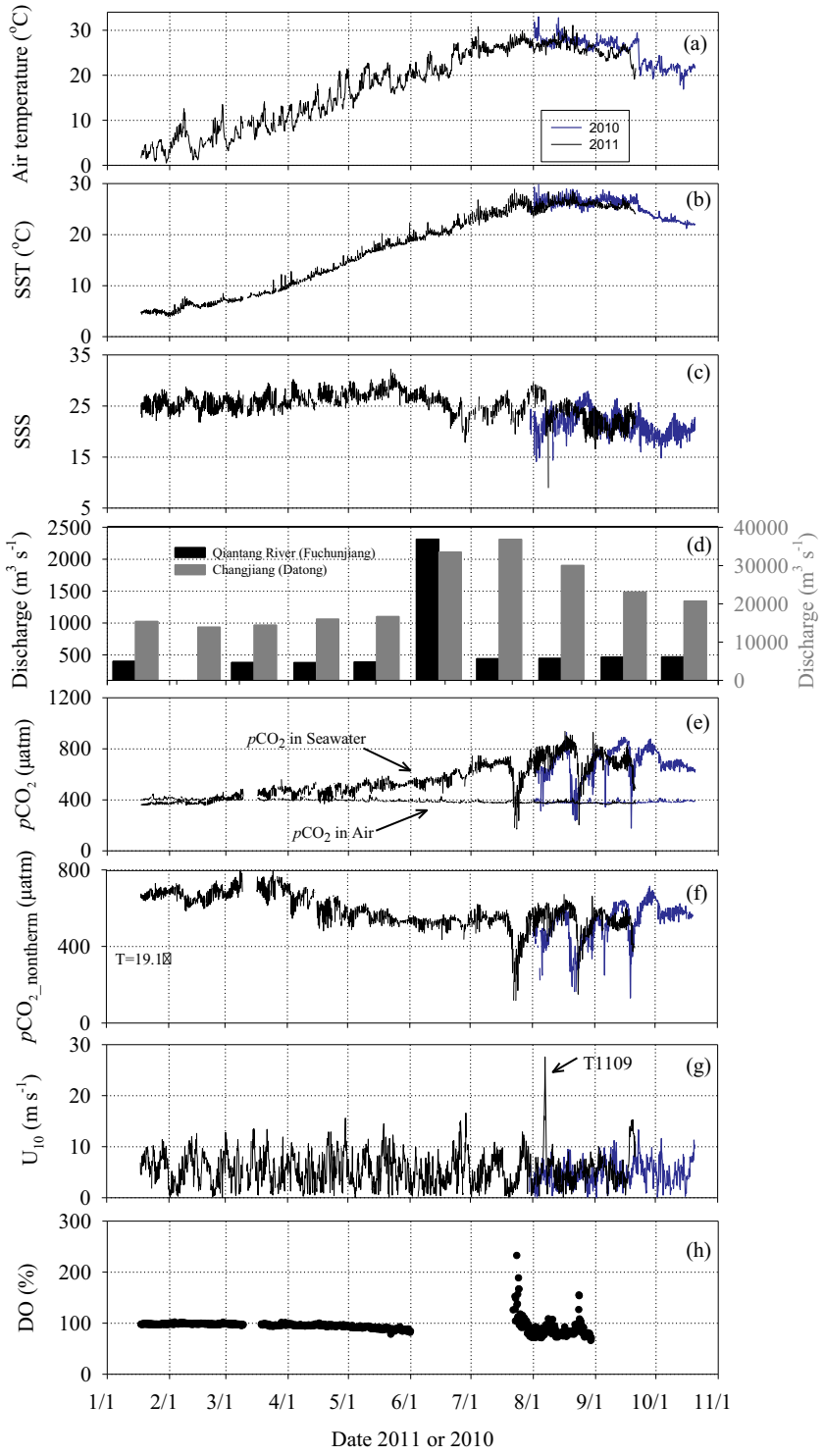

Fig. 3. Time-series observations of atmospheric temperature (a), sea surface temperature (b), sea surface salinity (c), monthly discharges of the Changjiang (Datong Gauge station) and Qiantang River (Fuchunjiang Gauge station) (d), sea surface pCO_2 (e), temperature-normalized sea surface pCO_2 ($pCO_{2\_nontherm}$, normalized to 19.1 °C) (f), wind speed at height of 10 m above sea surface (g), and dissolved oxygen (DO) saturation (h) at the bouy from August 2010 to September 2011. Blue and black lines represent data from 2010 and 2011, respectively. The high wind speeds were observed on August 6 and 7, 2011 with the influence of a typhoon, MUIFA, T1109 (g). Note that data are lacking from October 21, 2010 to January 16, 2011 due to the buoy's maintenance work. (For interpretation of the references to colour in this figure legend, the reader is referred to the web version of this article.)

seasonal variations, with a maximum value of 407 ± 8 μatm in winter and a minimum value of 379 ± 7 μatm in summer (Fig. 3e), which agrees well with seasonal fluctuations of atmospheric CO_2 background values measured on land (30°18′ N, 119°44′ E, 250 km away from our study site) (Pu et al., 2011). The average atmospheric pCO_2 value during the study period in 2011 was 392 ± 14 μatm, which was in consonance with the global level that year (Le Quéré et al., 2018). It should be noted that sea surface pCO_2 started to decrease in October 2010 compared to summer, but due to lack of sufficient data this study did not intend to assess the variability of pCO_2 and its controlling factors in fall. When the temperature effect was removed, the seasonal increase trend disappeared. The highest $pCO_{2\_nontherm}$ existed around winter from January to the early of April, but the variability pattern of $pCO_{2\_nontherm}$ kept consistent with pCO_2 in summer, and the minimum $pCO_{2\_nontherm}$ still occurred in summer.

There are no significant monthly variations in wind speed except on

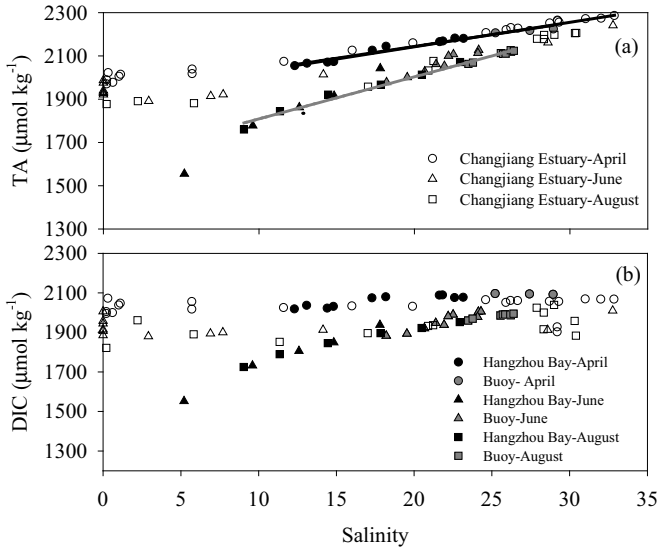

Fig. 4. Total alkalinity (TA) versus salinity (a) and dissolved inorganic carbon (DIC) versus salinity (b) in the Changjiang Estuary, Hangzhou Bay, and at the buoy site sampled during April, June, and August 2011. The straight lines in Panel (a) indicate conservative mixing in spring (April) and summer (June and August), respectively.

August 6 and August 7, 2011, when the wind speed was very high due to the influence of a typhoon (MUIFA, T1109, Fig. 3g).

DO saturation state was constant at around 100% from January 17 to May 31, 2011, but ranged from 66% to 232% during July 22 to August 22, 2011.

TA generally behaves conservatively, which makes it a plausible tracer of water mass mixing (Zhai et al., 2007). TA correlated well with salinity in Hangzhou Bay, including at the buoy site, during the cruises conducted in April, June, and August of 2011 (Fig. 4a). In April, TA in Hangzhou Bay and the Changjiang Estuary generally followed the same mixing line. Considering the much greater discharge of the Changjiang River compared to the Qiantang River (~30 fold higher) in April (Fig. 3d), during this time the buoy site was dominated by mixing of two water masses from the Changjiang plume and ECS. However, in June and August the TA mixing line in Hangzhou Bay largely deviated from the Changjiang Estuary, suggesting a significant contribution from the Qiantang River (discharge ~2316 m s^{-1} in June) to the buoy site in summer. This may be due to the fact that the core of the Changjiang plume turns northeast after leaving the Changjiang Estuary in summer when it can hardly influence the buoy site.

3.2. Seasonal variations of surface seawater pCO_2

The average pCO_2 and related parameters in different seasons are shown in Table 1. It should be noted that we only used the 2011 data to calculate the average seasonal values. The average SST increased from winter to spring to summer, with values of 5.7 ± 0.9 °C, 15.0 ± 4.8 °C, and 25.5 ± 1.1 °C, respectively. SSS during these three seasons was 25.4 ± 1.4, 26.5 ± 1.9, and 23.5 ± 2.5, respectively. Tidal range was constant during these seasons with values of 2.90 ± 0.8 m in winter, 2.78 ± 0.8 m in spring, and 2.80 ± 0.8 m in summer. Sea surface pCO_2 showed large seasonal changes that followed temperature variations, with the highest pCO_2 values observed in summer (687 ± 110 μatm), the lowest in winter (382 ± 18 μatm), and medium values in the spring (500 ± 56 μatm). The overall range in average pCO_2 values among seasons was 305 ± 111 μatm (Fig. 7). Average DO saturation levels were nearly saturated in winter (98% ± 1%) and spring (94% ± 4%), but undersaturated and variable in summer (89% ± 20%).

Table 1
Seasonal variations in sea surface salinity (SSS), sea surface temperature (SST), tidal range, dissolved oxygen (DO) satuation, pCO_2 in surface seawater, atmospheric pCO_2, wind velocity, and air-sea CO_2 exchange fluxes at the study site.

Period	Season	SSS	SST (°C)	Tidal range (m)	DO (%)	Sea surface pCO_2 (μatm)	Atmospheric pCO_2 (μatm)	Wind velocity (m s^{-1})	CO_2 flux[a] (mmol m^{-2} d^{-1})
2011/1/18-2/28 (41 days)	Winter	25.4 ± 1.4	5.7 ± 0.9	2.90 ± 0.8	98 ± 1	382 ± 18	407 ± 8	5.7 ± 2.9	−3 ± 2
2011/3/1-6/30 (108 days)	Spring	26.5 ± 1.9	15.0 ± 4.8	2.78 ± 0.8	94 ± 4	500 ± 56	396 ± 10	5.5 ± 3.1	10 ± 13
2011/7/1-9/20 (82 days)	Summer	23.5 ± 2.5	25.5 ± 1.1	2.80 ± 0.8	89 ± 20	687 ± 110	379 ± 7	5.4 ± 3.3	30 ± 27

Error bars represent standard deviations of temporal variability.
[a] gas transfer velocity of CO_2 was calculated from Sweeney et al. (2007).

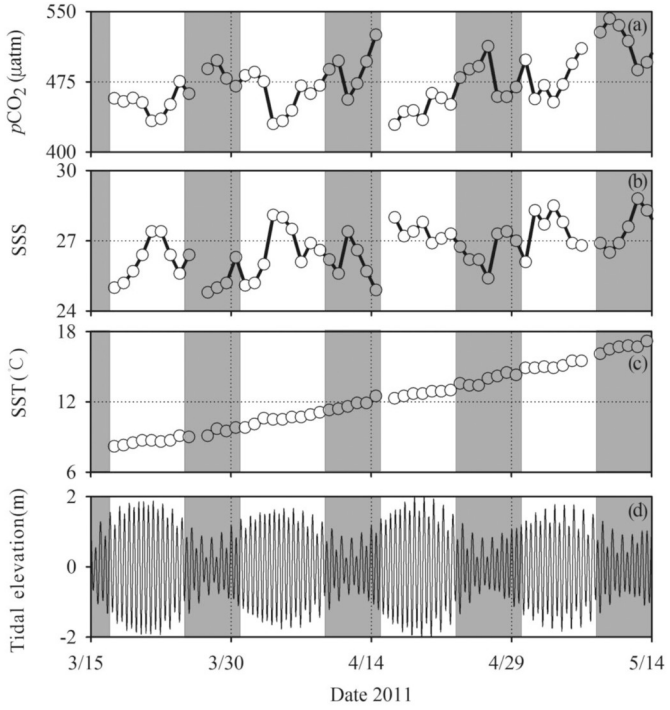

Fig. 5. Variations in daily-averaged sea surface pCO_2 (a), sea surface salinity (SSS) (b), sea surface temperature (SST) (c), and tidal elevation (d) in spring (March 15 to May 14, 2011) at the mooring site. Shaded areas denote neap tide periods.

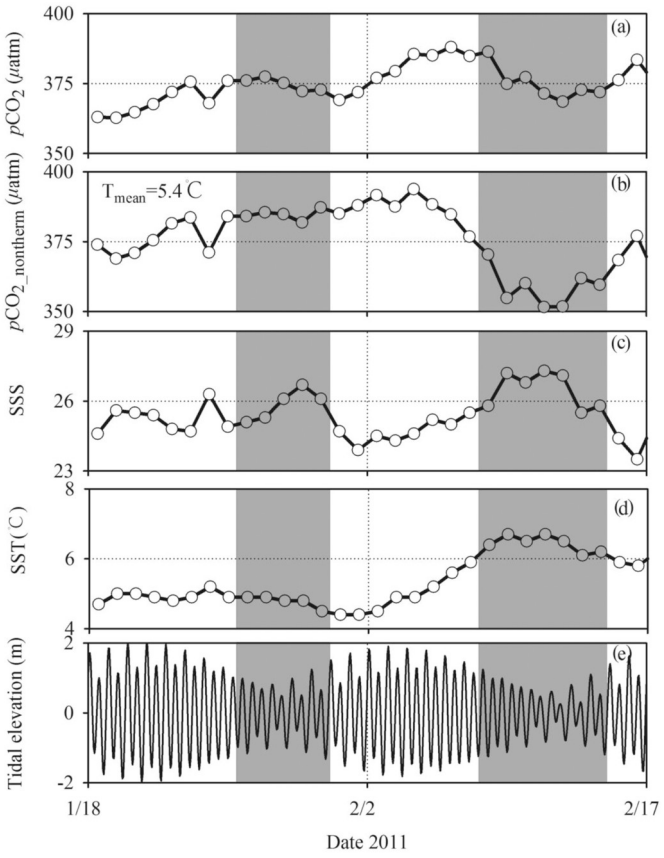

Fig. 6. Variations in daily-averaged sea surface pCO_2 (a), temperature-normalized sea surface pCO_2 (pCO_2_nontherm) (b), sea surface salinity (SSS) (c), sea surface temperature (SST) (d), and tidal elevation (e) in winter (January 18 to February 17, 2011) at the mooring site. Gray shaded areas represent neap tide periods.

3.3. Surface seawater pCO_2 variability of intra-seasonal scales (spring-neap/neap-spring tide)

Variations in daily-averaged SSS in spring and summer were roughly larger during spring tides and smaller during neap tides (Fig. 5b; Appendix Figs. S1c, S2b), although this was not the case in winter (Fig. 6c). Daily-averaged sea surface pCO_2 in spring together with temperature-normalized pCO_2 ($pCO_{2\_nontherm}$) in winter generally had an inverse relationship with SSS (Fig. 5a, b; Fig. 6b, c). Large variability of daily-averaged SST existed in spring (~9 °C) as compared to that in winter (~2 °C) and summer (3–4 °C) (Figs. 5c, 6d; Appendix Figs. S1d, S2c). Small variations in daily-averaged sea surface pCO_2 were observed in winter, with amplitudes in spring-neap/neap-spring cycles ranging from 15 to 57 μatm (average 30 ± 18 μatm) (Fig. 7). In spring, they ranged from 35 to 96 μatm (average 65 ± 22 μatm) (Fig. 7). In summer, daily-averaged sea surface pCO_2 showed distinct declines during neap tides, with the minima of pCO_2 reaching below the level in the air (Appendix Figs. S1a, S2a). The largest pCO_2 amplitudes were observed in summer, ranging from 52 to 480 μatm with an average of 283 ± 139 μatm (Fig. 7), similar to the average seasonal variation range of 305 ± 111 μatm (Fig. 7).

3.4. Diurnal variability of surface seawater pCO_2

The study site showed a regular semidiurnal tide, and the daily tidal range decreased from ~ 4 m at spring tides to ~ 2 m at neap tides. The diurnal amplitude of SST in winter, spring, and summer was from 0.5 to 1.2 °C, 0.2 to 1.6 °C, and 0.2 to 2.6 °C, respectively. Variations in SSS generally correlated with tidal cycles, with lower values observed during low tides and higher values coinciding with high tides (Appendix Fig. S3b, c, Fig. S4b, c, and Fig. S5b, d). Sea surface pCO_2 was significantly inversely correlated with SSS in both winter and spring (Appendix Fig. S3a, b, and Fig. S4a, b). Diurnal variability of pCO_2 during the spring tide in summer followed the same trend as in winter and spring, while it tended to be consistent with day-night cycles

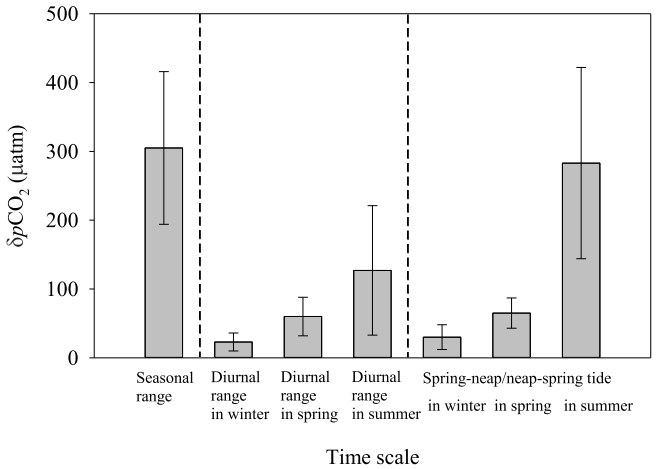

Fig. 7. Variation in ranges of sea surface pCO_2 (δpCO_2) at the seasonal, diurnal, and spring-neap/neap-spring scale in winter, spring, and summer. Error bars are standard deviations, which characterize the temporal variability rather than analytical errors in the measurement of sea surface pCO_2.

during neap tides, with the minima occurring at ~18:00 h (Beijing Time) and generally rising at night (Appendix Fig. S5a, b). The diurnal amplitudes of sea surface pCO_2 in winter, spring, and summer ranged from 6 to 56 μatm (average 23 ± 13 μatm) (Fig. 7), 15 to 162 μatm (60 ± 28 μatm) (Fig. 7), and 16 to 636 μatm (average 127 ± 94 μatm)

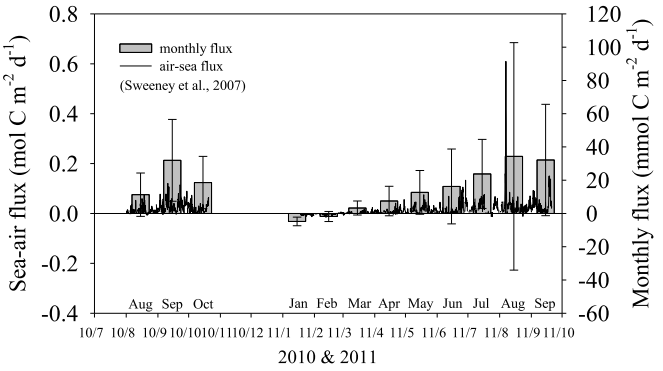

Fig. 8. Daily and monthly sea-air CO_2 fluxes at the mooring site from August to October 2010, and January to September 2011. Positive values represent CO_2 degassing. The monthly flux equaled the average value from the first day to last day of the month with the exception of October (from 1st-20th, 2010), January (from 17th-31st, 2010), and September (from 1st-20th, 2011). Error bars are standard deviations, which characterize the temporal variations in fluxes.

(Fig. 7), respectively. Summer had much larger diurnal variations in pCO_2 relative to winter and spring (Fig. 7).

4. Discussion

4.1. Air -sea CO_2 exchange flux

Sea surface pCO_2 was above atmospheric pCO_2 levels most of the time (from March to September 2011 and August to October 2010), with the exception of winter and part of the summer (Fig. 3e). It is thus clear that the study site was overall a source of CO_2 for the atmosphere, with an average air-sea flux of 14 ± 9 mmol C m^{-2} d^{-1} from January to October 2011. In winter, the study area was a sink of atmospheric CO_2 with an average air-sea flux of −4.8 ± 3 mmol C m^{-2} d^{-1} in January and − 1.8 ± 3 mmol C m^{-2} d^{-1} in February (Fig. 8). Although the sharp drop of surface water pCO_2 appeared in summer (July and August 2011, August and September 2010), the average air-sea flux was ~ 3-fold higher in summer vs. in spring of 2011 (30 ± 26 vs. 9.9 ± 7 mmol C m^{-2} d^{-1}). Since there are no significant monthly variations in wind speed, the monthly variability of air-sea flux is dominated by the ΔpCO_2 (difference between surface seawater pCO_2 and atmospheric pCO_2).

4.2. Controls on seasonal variations in surface water pCO_2

Sea surface pCO_2 in nearshore systems is modulated by a variety of factors including temperature, tidal mixing and biological activity, etc. Temperature affects sea surface pCO_2 through changing the thermodynamic conditions of the carbonate system, and tides determine sea surface pCO_2 through mixing of different water masses. Biological processes may include photosynthesis, respiration and calcium carbonate precipitation or dissolution, which alter the mass balance of the carbonate system and thus affect pCO_2 in seawater (Dai et al., 2009).

Temperature typically dominates the seasonal variations in sea surface pCO_2 in many previous studies (Bates et al., 1998; Nemoto et al., 2009; Turk et al., 2010; Lu et al., 2011). In this study, thermally affected pCO_2 (pCO_{2therm}) was generally consistent with the distribution of pCO_2 (Fig. 9a) except in summer, clearly suggesting that temperature was a principal factor in controlling the seasonal variations in pCO_2. A large deviation between measured pCO_2 and thermally affected pCO_2 was observed in some days in summer (July, August, and September), and this dramatic drawdown might be influenced by strong biological uptake. Additionally, horizontal mixing could be another important driving factor leading to seasonal variations in pCO_2, which could be evidenced by a strong correlation between temperature-normalized pCO_2 ($pCO_{2\_nontherm}$) and sea surface salinity ($p < .0001$, Fig. 9b) in winter (January, February) and spring (March, April, and May). Exceptions existed in summer, as insignificant relationships were observed in June ($R^2 = 0.003$, $p = .48$) and July ($R^2 = 0.09$, $p = .47$) of 2011 (Fig. 9b). In addition, winter had higher $pCO_{2\_nontherm}$ values compared to summer (Figs. 3f and 9b). The estimated pCO_2 in bottom water was higher than that at the surface water in August (Appendix Fig. S6). Therefore, the greater $pCO_{2\_nontherm}$ in winter might be explained by CO_2-enriched bottom water mixing with surface water due to winter cooling and monsoonal winds, together with strong biological activity in summer. The measured DIC concentration in April was higher than that in June and August at the mooring site (Fig. 4b), which also support the notion.

4.3. Controls on intra-seasonal variations in surface water pCO_2

The amplitude of pCO_2 induced by temperature (δpCO_{2_therm}) was minor compared to non-temperature affected pCO_2 amplitudes ($\delta pCO_{2\_nontherm}$) in the summers of 2010 and 2011 (Fig. 10c, d). However, in winter and spring, temperature could be one important factor that changes surface water pCO_2 (Fig. 10a, b).

The generally mirrored relationship found between pCO_2 and SSS in winter and spring demonstrated that mixing of water masses may have contributed greatly to the variations in pCO_2 of these two seasons (Figs. 6b, c and 5a, b). The positive correlations between $pCO_{2\_nontherm}$ and DO in winter and spring (Fig. 11) suggested that biological metabolism played a minor role in changing pCO_2. In winter, both $pCO_{2\_nontherm}$ and DO have good correlations with SSS (Fig. 9b, Appendix Fig. S7), and the ratio between the slope of $pCO_{2\_nontherm}$ vs. SSS (−8.0) and slope of DO vs. SSS (−5.7) was around 1.4, which was comparable with the slope between $pCO_{2\_nontherm}$ and DO (1.44), indicating that water masses mixing dominated the variations of $pCO_{2\_nontherm}$ and DO in winter.

To quantify the various pCO_2 controlling factors, we constructed a mass balance model based on Xue et al. (2016), with the details presented in Appendix S1. We applied the budget model to April 3–30 which represents spring. Fig. 12 shows the overall pCO_2 change and contributions from temperature effects, air-sea exchange, water mass mixing, biological metabolism, and residual term (mainly reflecting the sum of contributions of any factors not listed, such as diffusion, carbonate mineral dissolution/formation) during the target periods. In April, temperature was the predominant controlling factor affecting pCO_2, leading to a 85 ± 9 μatm rise in pCO_2 as the water temperature increased by 4.2 °C. pCO_2 variations as a function of temperature in April matched well with the pCO_{2therm} curve (Fig. 9a). Moreover, horizontal mixing between nearshore and offshore water also played a significant role in contributing to pCO_2 variability (41 ± 14 μatm). We assumed the salinity differences were solely attributed to mixing processes, as a strong correlation ($R^2 = 0.66$, $P < .0001$) observed between $pCO_{2\_nontherm}$ and salinity in April (Fig. 9b) validates the importance of water mass mixing. In summary, temperature, mixing, and air-sea exchange were the major controlling factors, contributing respectively 51%, 20%, and − 20% to the absolute pCO_2 change in April.

In spring, significant positive correlations occurred between daily-averaged $pCO_{2\_nontherm}$ and DO (Fig. 11) with a slope 1.8. Like in winter, strong correlations also existed between $pCO_{2\_nontherm}$ vs. SSS, and DO vs. SSS in spring (Appendix Fig. S7). However, the ratio between the slope of $pCO_{2\_nontherm}$ vs. SSS (−37.0) and slope of DO vs. SSS (−12.1) was 3.0, higher than the slope of 1.8. This discrepancy might be explained by the different effect of air-sea exchange on the variability of $pCO_{2\_nontherm}$ and DO in spring. Therefore, although we observed positive correlations between $pCO_{2\_nontherm}$ and DO in both spring and winter (Fig. 11), water masses mixing and air-sea exchange drive the variation of $pCO_{2\_nontherm}$ in spring; in winter the $pCO_{2\_nontherm}$ is mainly controlled by water masses mixing.

In summer, a negative correlation was found between $pCO_{2\_nontherm}$

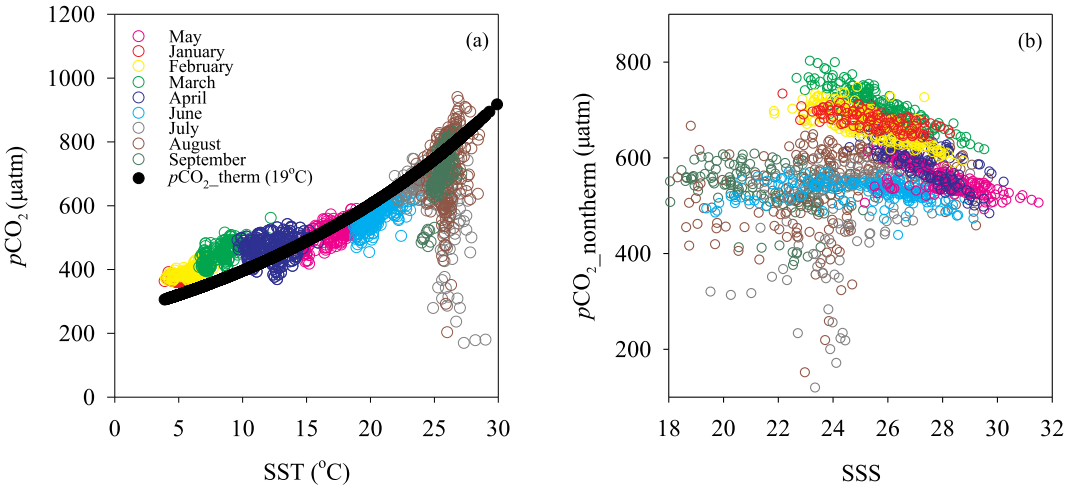

Fig. 9. Sea surface pCO_2 versus sea surface temperature (SST) (a), temperature-normalized sea surface pCO_2 ($pCO_{2\_nontherm}$, normalized to 19.1 °C) versus sea surface salinity (SSS) (b) in 2011. A strong correlation between $pCO_{2\_nontherm}$ and SSS in winter ($p < .0001$, January and February) and spring ($p < .0001$, March, April, and May). However, insignificant relationships were observed in June ($p = .48$) and July ($p = .47$) of 2011.

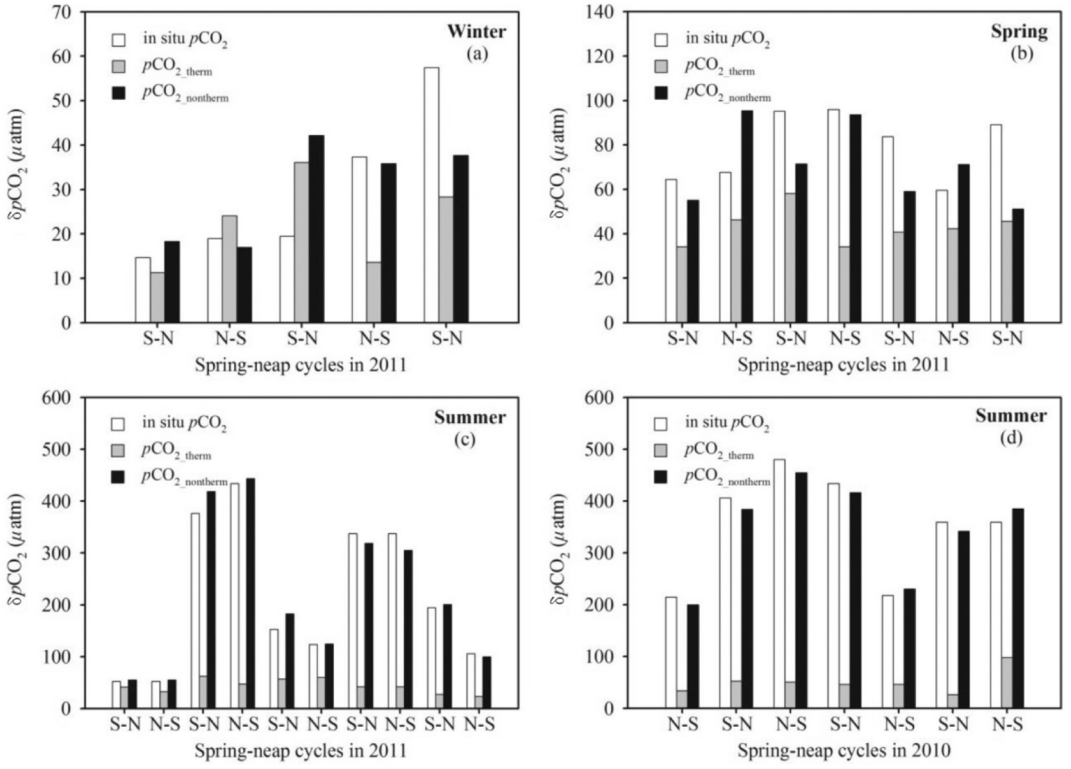

Fig. 10. The amplitude of sea surface pCO_2, pCO_{2_therm}, and $pCO_{2\_nontherm}$ during spring-neap and neap-spring tidal cycles in winter (January 18 to February 28) (a), spring (March 15 to May 14) (b), summer 2011 (July 1 to September 21) (c), and summer 2010 (August 1 to September 30) (d) at the mooring site.

and DO concentration, with a Pearson coefficient of 0.84 ($P < .1$, Fig. 11) and a slope of −2.9, which means a 1 µmol kg^{-1} increase in DO can reduce pCO_2 by ~3 µatm. This is comparable with the organic metabolism effect, of which a 1 µmol kg^{-1} variation of DO can cause an ~4 µatm inverse variation in pCO_2. Consequently, photosynthesis and respiration might be the predominant mechanism controlling the spring-neap variations in pCO_2 in summer. Daily-averaged sea surface turbidity observed at the study site in summer (2011) ranged from 5 to 220 NTU, which corresponded to 6–320 mg L^{-1} of TSM in terms of the relationship reported by He et al. [He et al., 2013, TSM (mg L^{-1}) = −0.72 + 1.45 × turbidity (NTU)]. High concentrations of suspended particles lead to high turbidity and low light transmittance, and thus photosynthetic production was likely to be limited by light (Ning et al., 1988; Cai et al., 2002). In general, TSM concentrations were higher in winter than in summer (Chen et al., 2006a,b) because in summer resuspension is weakened by increasing riverine discharge. Chen et al. (2006a,b) conclude that tide-induced sediment resuspension ultimately controls the concentration of TSM. It has also been found that photosynthesis is enhanced when the concentration of TSM is < 10 mg L^{-1} in the plumes of the Changjiang and Amazon River (DeMaster et al., 1986; Ning et al., 1988; DeMaster and Pope, 1996). At our study site, we did not measure Chl *a* during 2010–2011. Instead, we used the sensor data of Chl *a*, turbidity (a FLNTU Combination Fluorometer and Turbidity Sensor) and pCO_2 deployed in another buoy

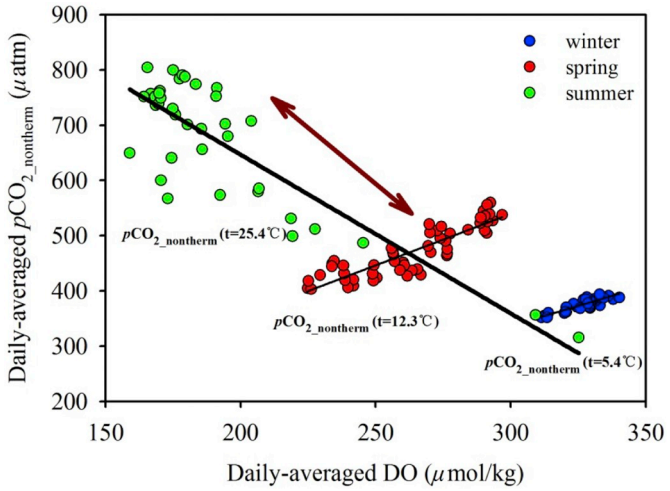

Fig. 11. Daily-averaged $pCO_{2\_nontherm}$ vs daily-averaged dissolved oxygen (DO) at the mooring site in winter (January 18 to February 17), spring (March 19 to May 14), and summer (July 23 to August 29), 2011. Black lines are the regression lines of these three seasons. The double arrow line denotes the pCO_2 variation trend with DO following classic Redfield Stoichiometry.

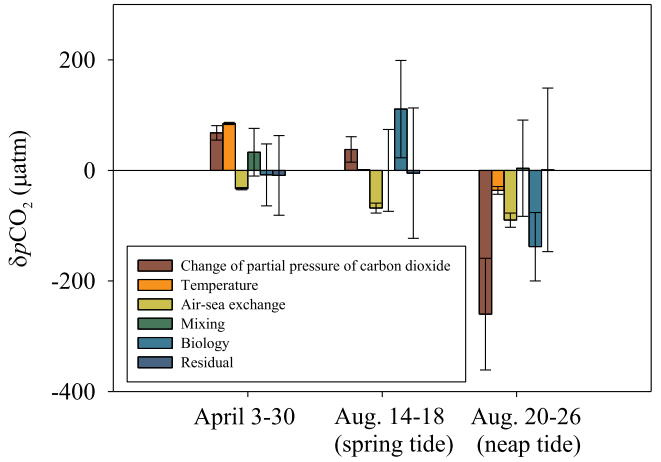

Fig. 12. Variations in pCO_2 (δpCO_2) and term contributions from temperature, sea-air CO_2 exchange, horizontal mixing, biological activity, and residual terms during April 3–30, August 14–18 (spring tide), and August 20–25 (neap tide), 2011.

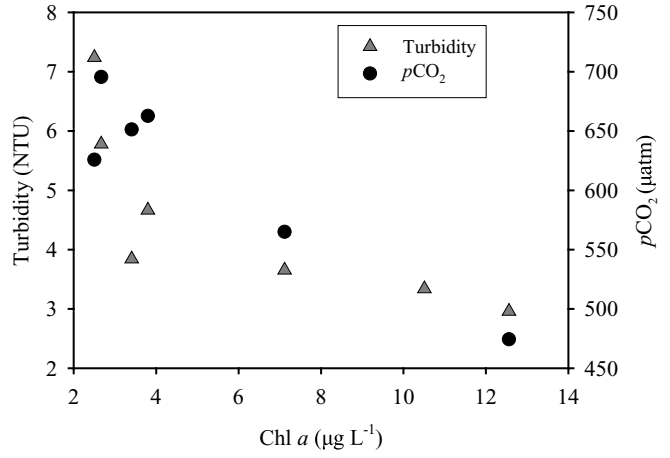

Fig. 13. Turbidity versus chlorophyll a (Chl a) and pCO_2 versus Chl a in surface seawater at the mooring site sampled on July 26, 2012.

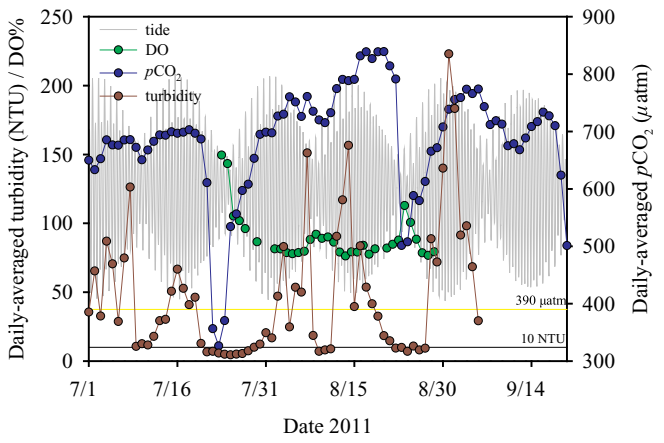

Fig. 14. Tidal height variations and daily-averaged turbidity, dissolved oxygen (DO) saturation, and pCO_2 at the mooring site sampled from July 1 to September 20, 2011. Yellow line is for atmospheric pCO_2. (For interpretation of the references to colour in this figure legend, the reader is referred to the web version of this article.)

system at the same site in July 2012, which indicated that when turbidity was < 10 NTU, Chl a increased and pCO_2 was reduced dramatically along with the decline in turbidity (Fig. 13). During the neap tides of summer 2011, turbidity was nearly 10 NTU or less, and sea surface pCO_2 at the site exhibited a significant drawdown, at times even becoming lower than atmospheric pCO_2 (Fig. 14). Meanwhile, DO saturation rate showed a large increase, at times even appearing to be supersaturated (Fig. 14). An algal bloom was observed near the buoy site during neap tide on August 22–24, 2011 (Liu, 2014), corresponding with a remarkable decrease in both pCO_2 and turbidity. Generally, turbidity fluctuated with the tidal cycles, with high values during spring tides and low values during neap tides (Fig. 14). During spring tides, high turbidity resulted from strong current velocities and associated sediment resuspension. The mass balance model was separately applied to August 20–25 (neap tide in summer) when the algal bloom occurred, and to August 14–18 (spring tide in summer). During the spring tide in August, biological activity was the main driver of changes in surface water pCO_2, which resulted in pCO_2 increases as high as 123 ± 49 µatm (Fig. 12), 60% of the total pCO_2 change, suggesting respiration exceeded photosynthesis. The net community production (NCP) in the mixed layer was estimated to −17 ± 10 mmol m^{-2} d^{-1}. The negative value suggests that this site was heterotrophic during August 14–18. The calculation method of NCP was presented in Appendix S1. Based on in situ incubation experiments conducted during the August 2011 cruise, the respiration rate was greater than primary productivity (Liu, 2014): i.e. the system was heterotrophic, supporting our model results. Similar results were also observed near our study area in June and August 2003 (Chen et al., 2006a,b). As opposed to other seasons, air-sea CO_2 exchange significantly decreased pCO_2 by 68 ± 9 µatm (Fig. 12), accounting for −37% (degassing) of the total pCO_2 change, since sea surface pCO_2 was extremely high with an average value of 815 ± 23 µatm during spring tide in August. During the algal bloom event, which occurred at an August neap tide, we observed a dramatic decline in sea surface pCO_2 (with an average of 260 ± 130 µatm for sea surface pCO_2), which can largely be explained by the amplified primary production. Consistently, the model result showed that biological production was the greatest contributor (123 ± 56 µatm, −51% of the absolute pCO_2 change, Fig. 12) to the decrease in pCO_2. The mean NCP in the mixed layer during this period was 18 ± 9 mmol m^{-2} d^{-1}, much higher than that in April which was 0.2 ± 10 mmol m^{-2} d^{-1}. In addition, CO_2 degassing reduced pCO_2 by 90 ± 10 µatm (Fig. 12), −33% of the absolute pCO_2 change, suggesting that air-sea exchange also had an important effect on the CO_2 decline. Overall, horizontal mixing was

a minor factor altering pCO_2 in August. A weak relationship existed between temperature-normalized pCO_2 and salinity in August ($R^2 = 0.07$, Fig. 9b), supporting our model result.

4.4. Controls of the diurnal variations in surface seawater pCO_2

Temperature-induced diurnal variations in sea surface pCO_2 (pCO_{2_therm}) were smaller than those caused by non-temperature effects ($pCO_{2\_nontherm}$) during all seasons (Appendix Fig. S9), particularly in spring, suggesting that temperature had a limited effect on the diurnal variations in sea surface pCO_2.

In this study, sea surface pCO_2 showed an inverse correlation with tidal height during winter, spring and spring-tides in summer, implying that tide-induced mixing between nearshore water (high pCO_2) and offshore ECS water (low pCO_2) likely dominate the diurnal variations in sea surface pCO_2. The diurnal amplitudes of sea surface pCO_2 observed in winter and spring showed good correlations with SSS, with Pearson correlation coefficients of 0.88 and 0.89, respectively ($n = 7$, $P < .1$). This again suggests that tide-induced water mixing at our site played the most important role on the diurnal variations in surface pCO_2. Tidal mixing dominated the variations in sea surface pCO_2 as has also been observed in Shenhu Bay and Xiamen Bay (Dai et al., 2009). It should be noted that diurnal amplitudes of pCO_2 had insignificant or weaker correlations with diurnal tidal amplitudes in winter and spring, which might be explained by sporadic effects of the river plumes in addition to tidal-driven water mass mixing.

A typical biological cycle (photosynthesis and respiration) would lead to sea surface pCO_2 drawdown during the day and increases at night, typically with mirrored variations in DO (Dai et al., 2009; Jiang et al., 2011). In the present study, neither biology-induced pCO_2 variability nor significant inverse correlations between pCO_2 and DO were observed in winter and spring, suggesting that photosynthesis and respiration may have little effect on the diurnal variations in sea surface pCO_2 during these two seasons. However, there was one exception. During the neap tides of summer, diurnal variability in pCO_2 was consistent with day-night cycles and mirrored DO variations.

4.5. Controls on the inter-summer variation in surface water pCO_2

During the buoy mooring period, two full months of August were covered in 2010 and 2011. The corresponding monthly air-sea fluxes were 11 ± 13 and 34 ± 69 mmol C m^{-2} d^{-1}, respectively. Extremely high variability (± 69) was observed in August 2011, which was mainly due to high wind speeds on August 6 and 7 resulting from the influence of a typhoon. If we remove these two high wind speed days, the monthly air-sea flux estimate is reduced to 21 ± 17 mmol C m^{-2} d^{-1} in August 2011, which is still greater than that estimated for August 2010 according to a *t*-test ($p < .05$). The higher CO_2 exchange flux in August 2011 was caused by the high sea surface pCO_2 values and wind speeds in 2011 relative to 2010 (727 ± 110 vs. 619 ± 135 μatm), since comparable atmospheric pCO_2 and sea surface temperatures were observed during these two months. Detailed monthly values are shown in Table 2.

Comparing surface pCO_2 variations in August 2010 with August 2011 (Fig. 3e), we notice a drastic reduction in surface pCO_2 occurring on August 4–6, 20–21, 30–31, 2010, and August 23–24, 2011, all of which occurred during neap tides. August 2011 covered two neap tides, although one was affected by a typhoon, while August 2010 included ca. three neap tides, indicating stronger tidal currents existed in August 2011. If these low surface water pCO_2 values during neap tide are excluded, the surface pCO_2 was still significantly greater in August 2011 compared with August 2010, verified by *t*-test. The recalculated monthly average surface pCO_2 values are 696 ± 76 and 763 ± 71 μatm during August 2010 and 2011, respectively. In addition, if we assume SSS primarily represents riverine inputs, the lower SSS values (by 1.2 units) in August 2010 compared to August 2011 suggests higher river flows in August 2010. Consistently, the measured river discharge from the Changjiang at the Datong gauge station was greater in August 2010 than in August 2011. As shown in Section 4.3, TSM concentrations increase with strong tidal current velocities and lower river flows. TSM concentrations were retrieved from the obtained remote sensing reflectance based on the regional retrieval algorithm (He et al., 2013). Because of the heavy influence of clouds on the daily product, all daily products were merged into a monthly product as shown in Appendix Fig. S10. Here, we can see the TSM concentration was lower in August 2010 than in August 2011. Due to light limitation at the buoy site, it is mostly heterotrophic; lower TSM during neap tides would enhance biological uptake and drawdown surface pCO_2. Horizontal mixing was an insignificant factor altering sea surface pCO_2 in summer (Chen et al., 2008). Here, we ruled out the influence from mixing between the high pCO_2 Changjiang River and low pCO_2 offshore seawater. Therefore, the relatively lower sea surface pCO_2 in August 2010 was likely due to enhanced biological production, resulting from the lower turbidity driven by weak tidal currents and high river flows. Contrary results have been reported in the central South Atlantic Bight, which had higher aqueous pCO_2 values and river fluxes from September–October 2007 compared with September–October 2006. This high surface pCO_2 in fall 2007 is largely explained by enhanced decomposition of organic matter carried by saltmarshes and estuaries during increases in river flows (Xue et al., 2016). Moreover, in August 2010, under-sampling during neap tides would lead to a 12% increase in average surface pCO_2 estimates and a 21% increase in estimated CO_2 exchange fluxes. As a consequence, to avoid overestimating sea-to-air CO_2 exchange fluxes in the Hangzhou Bay nearshore system, it is important to thoroughly characterize periods of low turbidity during neap tides.

5. Conclusions

The yearly continuous high frequency observations of sea surface pCO_2 were conducted near the mouth of Hangzhou Bay (Outer Changjiang Estuary) from July 30 to October 20, 2010, and January 17 to September 20, 2011. Highly variable seawater pCO_2 was observed over different timescales, ranging from seasonal to short-term scales. Over spring-neap and diel timescales, the mean amplitudes of seawater pCO_2 were the lowest in winter, had medium values in spring, and the highest in summer. The mean amplitude of daily-averaged sea surface pCO_2 during the summer was comparable to the pCO_2 amplitude at the seasonal scale (283 ± 139 vs 305 ± 111 μatm). In winter, this site

Table 2
Comparison of monthly surface water pCO_2 and other parameters during August 2010 and August 2011 at the buoy site. Error bar represents one standard deviation.

Month	SSS	SST(°C)	Sea surface pCO_2 (μatm)	Atmospheric pCO_2 (μatm)	Wind velocity (m s^{-1})	CO_2 flux[a] (mmol m^{-2} d^{-1})	Changjiang flux[b] (m^3 s^{-1})
August 2010	22.8 ± 2	26.6 ± 1	619 ± 135	380 ± 9	4.1 ± 0.4	11 ± 13	51,557
August 2011	24.0 ± 3	26.1 ± 1	728 ± 108 (727 ± 110)	380 ± 8	5.3 ± 4 (4.7 ± 2)	34 ± 69 (21 ± 17)	30,288

Values in parenthesis denote monthly averages without two days (August 6 and 7) which were affected by an episodic event (typhoon).
[a] Gas transfer velocity of CO_2 was calculated from Sweeney et al. (2007).
[b] The Changjiang flux was derived from the Datong gauge station (http://xxfb.hydroinfo.gov.cn/).

Table 3
Controlling factors on the variability of surface water pCO_2 at different time scales.

Time scales	Controlling factors
Seasonal range	Temperature, water masses mixing
Intra-seasonal scales (spring-neap/ neap-spring tide)	
Winter	Temperature, water masses mixing
Spring	Temperature, water masses mixing, air-sea exchange
Summer	Biological metabolism, air-sea exchange
Diurnal range	
Winter	Tidal mixing
Spring	Tidal mixing
Summer (spring-tide)	Tidal mixing
Summer (neap-tide)	Biological uptake
Inter-summer	Biological metabolism associated with turbidity

was a weak atmospheric CO_2 sink with an average air-sea exchange flux of -3.3 ± 2 mmol C m^{-2} d^{-1}. However, in spring and summer, it shifted from a CO_2 sink to a source, with averages air-sea CO_2 fluxes of 9.9 ± 7 and 30 ± 26 mmol C m^{-2} d^{-1}, respectively. Overall, the average sea surface pCO_2 value was 545 ± 138 μatm, and the air-sea CO_2 flux was estimated as 14 ± 9 mmol C m^{-2} d^{-1} during the observation period in 2011.

Driving factors that modulate seawater pCO_2 in nearshore systems generally include temperature, air-sea exchange, mixing, and biological process. The controlling factors at different time scales were presented in Table 3. Over seasonal timescales, temperature and mixing were the dominant controls on pCO_2 variability. Over spring-neap tidal cycle timescales, seawater pCO_2 negatively correlated with SSS in winter and spring, demonstrating the significant contribution from water mass mixing during these two seasons. In addition, temperature was also an important factor affecting pCO_2 in winter and spring. Based on mass balance models, temperature, mixing, and air-sea exchange were the major controlling factors, which generally supported our qualitative analysis. However, during the spring tides of August, biological metabolism and air-sea exchange were the dominant driving forces altering pCO_2. Over diurnal timescales, tide-induced mixing dominated the diurnal variations on surface pCO_2 in winter, spring, and during spring tides of summer. However, during the neap tides of summer, biological metabolism played an important role in the diurnal variability of surface pCO_2. Microtidal and low turbidity estuarine systems generally have lower surface seawater pCO_2 compared with macrotidal and highly turbid nearshore waters. For instance, the lower Neuse River estuary was found to be a CO_2 sink with a flux of -1.37 mmol m^{-2} d^{-1} (Crosswell et al., 2012), while our study site was a source of atmospheric CO_2, with high turbidity limiting biological production.

The low turbidity values were found during the neap tides of summer, corresponding with weak current velocities and high river flows at our study site. Relative to August 2011, August 2010 had comparable SST and lower SSS values, but significantly lower sea surface pCO_2 values. This lower pCO_2 (~100 μatm) during August 2010 was likely caused by enhanced biological uptake due to weak currents and increased river flows.

This study highlights the significance of tidal mixing and tidal phases on the variability of surface water pCO_2 from seasonal to diel scales. Even during the neap tides of summer, where biological activity dominates pCO_2 changes, the tidal phase in essence reduces turbidity and therefore enhances biological uptake. Temporal under-sampling could thus impact the evaluation of air-sea CO_2 fluxes. We contend that capturing the full tidal phase, particularly during periods of neap tide, is critically important for better understanding the processes and fluxes that govern air-sea CO_2 exchanges in the many macrotidal nearshore systems of the world.

Acknowledgements

This research was funded by the Ocean Public Welfare Scientific Research Project, State Oceanic Administration People's Republic of China through grant 201505003 (subtask No. 201505003-3). We thank Dr. Xianqiang He for providing the concentration of total suspended particulate matter retrieved from the remote sensing reflectance.

Appendix A. Supplementary data

Supplementary data to this article can be found online at https://doi.org/10.1016/j.marchem.2019.103690.

References

Le Quéré, C., Andrew, R.M., Friedlingstein, P., Sitch, S., Hauck, J., Pongratz, J., Pickers, P.A., Korsbakken, J.I., Peters, G.P., Canadell, J.G., Arneth, A., Arora, V.K., Barbero, L., Bastos, A., Bopp, L., Chevallier, F., Chini, L.P., Ciais, P., Doney, S.C., Gkritzalis, T., Goll, D.S., Harris, I., Haverd, V., Hoffman, F.M., Hoppema, M., Houghton, R.A., Hurtt, G., Ilyina, T., Jain, A.K., Johannessen, T., Jones, C.D., Kato, E., Keeling, R.F., Goldewijk, K.K., Landschützer, P., Lefèvre, N., Lienert, S., Liu, Z., Lombardozzi, D., Metzl, N., Munro, D.R., Nabel, J.E.M.S., Nakaoka, S.I., Neill, C., Olsen, A., Ono, T., Patra, P., Peregon, A., Peters, W., Peylin, P., Pfeil, B., Pierrot, D., Poulter, B., Rehder, G., Resplandy, L., Robertson, E., Rocher, M., Rödenbeck, C., Schuster, U., Schwinger, J., Séférian, R., Skjelvan, I., Steinhoff, T., Sutton, A., Tans, P.P., Tian, H., Tilbrook, B., Tubiello, F.N., van der Laan-Luijkx, I.T., van der Werf, G.R., Viovy, N., Walker, A.P., Wiltshire, A.J., Wright, R., Zaehle, S., Zheng, B., 2018. Global carbon budget 2018. Earth Syst. Sci. Data. 10, 2141–2194. https://doi.org/10.5194/essd-10-2141-2018.

Liu, J.W., 2014. On the Respiration and Ocean Acidificationin the Coastal Ocean. Ph.D Thesis (in Chinese). Xiamen University, Xiamen.

Bakker, D., Pfeil, B., Landa, C., Metzl, N., O'Brien, K., Olsen, A., Smith, K., Cosca, C., Harasawa, S., Jones, S., Nakaoka, S.I., Nojiri, Y., Schuster, U., Steinhoff, T., Sweeney, C., Takahashi, T., Tilbrook, B., Wada, C., Wanninkhof, R., Alin, S., Balestrini, C., Barbero, L., Bates, N., Bianchi, A., Bonou, F., Boutin, J., Bozec, Y., Burger, E., Cai, W.J., Castle, R., Chen, L., Chierici, M., Currie, K., Evans, W., Featherstone, C., Feely, R., Fransson, A., Goyet, C., Greenwood, N., Gregor, L., Hankin, S., Hardman-Mountford, N., Harlay, J., Hauck, J., Hoppema, M., Humphreys, M., Hunt, C., Huss, B., Ibánhez, J., Johannessen, T., Keeling, R., Kitidis, V., Körtzinger, A., Kozyr, A., Krasakopoulou, E., Kuwata, A., Landschützer, P., Lauvset, S., Lefèvre, N., Lo Monaco, C., Manke, A., Mathis, J., Merlivat, L., Millero, F., Monteiro, P., Munro, D., Murata, A., Newberger, T., Omar, A., Ono, T., Paterson, K., Pearce, D., Pierrot, D., Robbins, L., Saito, S., Salisbury, J., Schlitzer, R., Schneider, B., Schweitzer, R., Sieger, R., Skjelvan, I., Sullivan, K., Sutherland, S., Sutton, A., Tadokoro, K., Telszewski, M., Tuma, M., Van Heuven, S., Vandemark, D., Ward, B., Watson, A., Xu, S., 2016. A multi-decade record of high-quality fCO_2 data in version 3 of the Surface Ocean CO_2 Atlas (SOCAT). Earth Syst. Sci. Data. 8, 383–413. https://doi.org/10.5194/essd-8-383-2016.

Bates, N.R., Takahashi, T., Chipman, D.W., Knap, A.H., 1998. Variability of pCO_2 on diel to seasonal timescales in the Sargasso Sea near Bermuda. J. Geophys. Res. 103 (C8), 15567–15585. https://doi.org/10.1029/98JC00247.

Bauer, J.E., Cai, W.J., Raymond, P.A., Bianchi, T.S., Hopkinson, C.S., Regnier, P.A., 2013. The changing carbon cycle of the coastal ocean. Nature 504 (7478), 61–70. https://doi.org/10.1038/nature12857.

Beardsley, R.C., Limeburner, R., Yu, H., Cannon, G.A., 1985. Discharge of the Changjiang (Yangtze River) into the East China Sea. Cont. Shelf Res. 4, 57–76. https://doi.org/10.1016/0278-4343(85)90022-6.

Borges, A.V., Frankignoulle, M., 1999. Daily and seasonal variations of the partial pressure of CO_2 in surface seawater along Belgian and southern Dutch coastal areas. J. Mar. Syst. 19 (4), 251–266. https://doi.org/10.1016/S0924-7963(98)00093-1.

Bourgeois, T., Orr, J.C., Resplandy, L., Terhaar, J., Ethé, C., Gehlen, M., Bopp, L., 2016. Coastal-ocean uptake of anthropogenic carbon. Biogeosciences. 13, 4167–4185. https://doi.org/10.5194/bg-13-4167-2016.

Bozec, Y., Merlivat, L., Baudoux, A.C., Beaumont, L., Blain, S., Bucciarelli, E., Danguy, T., Grossteffan, E., Guillot, A., Guillou, J., Répécaud, M., Tréguer, P., 2011. Diurnal to inter-annual dynamics of pCO_2 recorded by a CARIOCA sensor in a temperate coastal ecosystem (2003-2009). Mar. Chem. 126 (1–4), 13–26. https://doi.org/10.1016/j.marchem.2011.03.003.

Caffrey, J.M., Chapin, T.P., Jannasch, H.W., Haskins, J.C., 2007. High nutrient pulses, tidal mixing and biological response in a small California estuary: variability in nutrient concentrations from decadal to hourly time scales. Estuar. Coast. Shelf Sci. 71 (3), 368–380. https://doi.org/10.1016/j.ecss.2006.08.015.

Cai, Y., Ning, X., Liu, Z., 2002. Studies on primary production and new production of the Zhujiang Estuary, China. in Chinese. Acta Oceanol. Sin. 24 (3), 101–111. https://doi.org/10.3321/j.issn:0253-4193.2002.03.014.

Cai, W.J., Dai, M.H., Wang, Y.C., Zhai, W.D., Huang, T., Chen, S.T., Zhang, F., Chen, Z.Z., Wang, Z.H., 2004. The biogeochemistry of inorganic carbon and nutrients in the Pearl River estuary and the adjacent Northern South China Sea. Cont. Shelf Res. 24 (12), 1301–1319. https://doi.org/10.1016/j.csr.2004.04.005.

Chen, C.C., Chiang, K.P., Gong, G.C., Shiah, F.K., Tseng, C.M., Liu, K.K., 2006a. Importance of planktonic community respiration on the carbon balance of the East China Sea in summer. Glob. Biogeochem. Cycles 20, GB4001. https://doi.org/10.1029/2005GB002647.

Chen, S.L., Zhang, G.A., Yang, S.L., Shi, J.Z., 2006b. Temporal variations of fine suspended sediment concentration in the Changjiang River estuary and adjacent coastal waters. China. J. Hydrol. 331 (1–2), 137–145. https://doi.org/10.1016/j.jhydrol.2006.05.013.

Chen, C.T.A., Zhai, W.D., Dai, M.H., 2008. Riverine input and air-sea CO_2 exchanges near the Changjiang (Yangtze River) Estuary: status quo and implication on possible future changes in metabolic status. Cont. Shelf Res. 28, 1476–1482. https://doi.org/10.1016/j.csr.2007.10.013.

Chen, C.T.A., Huang, T.H., Chen, Y.C., Bai, Y., He, X., Kang, Y., 2013. Air-sea exchanges of CO_2 in the world's coastal seas. Biogeosciences. 10, 6509–6544. https://doi.org/10.5194/bg-10-6509-2013.

Crosswell, J.R., Wetz, M.S., Hales, B., Paerl, H.W., 2012. Air-water CO_2 fluxes in the microtidal Neuse River Estuary, North Carolina. J. Geophys. Res.-Oceans. 117, C08017. https://doi.org/10.1029/2012JC007925.

Dai, A.G., Trenberth, K.E., 2002. Estimates of freshwater discharge from continents: latitudinal and seasonal variations. J. Hydrometeorol. 3, 666–687. https://doi.org/10.1175/1525-7541(2002)003<0660:EOFDFC>2.0.CO;2.

Dai, M.H., Lu, Z.M., Zhai, W.D., Chen, B.S., Cao, Z.M., Zhou, K.B., Cai, W.J., Chen, C.T.A., 2009. Diurnal variations of surface seawater pCO_2 in contrasting coastal environments. Limnol. Oceanogr. 54 (3), 735–745. https://doi.org/10.4319/lo.2009.54.3.0735.

DeMaster, D.J., Pope, R.H., 1996. Nutrient dynamics in Amazon shelf waters: results from AMASSEDS. Cont. Shelf Res. 16 (3), 263–289. https://doi.org/10.1016/0278-4343(95)00008-O.

DeMaster, D.J., Kuehl, S.A., Nittrouer, C.A., 1986. Effects of suspended sediments on geochemical processes near the mouth of the Amazon River: examination of biological silica uptake and the fate of particle-reactive sediments. Cont. Shelf Res. 6 (1/2), 107–125. https://doi.org/10.1016/0278-4343(86)90056-7.

Dickson, A.G., 1990. Standard potential of the reaction: $AgCl(s) + 1/2\ H_2(g) = Ag(s) + HCl(aq)$, and the standard acidity constant of the ion HSO_4^- in synthetic seawater from 273.15 to 318.15 K. J. Chem. Thermodyn. 22, 113–127.

Gao, X., Song, J., Li, X., Li, N., Yuan, H., 2008. pCO_2 and carbon fluxes across sea-air interface in the Changjiang Estuary and Hangzhou Bay. Chin. J. Oceanol. Limnol. 26 (3), 289–295. https://doi.org/10.1007/s00343-008-0289-8.

Gao, S.Q., Chen, J.F., Jin, H.Y., Wang, K., Lu, Y., Li, H.L., Chen, F.J., 2011. Characteristics of nutrients and eutrophication in the Hangzhou Bay and its adjacent waters (in Chinese with English abstract). J. Mar. Sci. 29 (3), 36–47.

Guo, X.H., Dai, M.H., Zhai, W.D., Cai, W.J., Chen, B.S., 2009. CO_2 flux and seasonal variability in a large subtropical estuarine system, the Pearl River Estuary. China. J. Geophys. Res. 114, G03013. https://doi.org/10.1029/2008JG000905.

Guo, X.H., Zhai, W.D., Dai, M.H., Zhang, C., Bai, Y., Xu, Y., Li, Q., Wang, G.Z., 2015. Air-sea CO_2 fluxes in the East China Sea based on multiple-year underway observations. Biogeosciences 12 (7), 5495–5514. https://doi.org/10.5194/bg-12-5495-2015.

He, X.Q., Bai, Y., Pan, D., Huang, N., Dong, X., Chen, J.S., Chen, C.T.A., Cui, Q.F., 2013. Using geostationary satellite ocean color data to map the diurnal dynamics of suspended particulate matter in coastal waters. Remote Sens. Environ. 133, 225–239. https://doi.org/10.1016/j.rse.2013.01.023.

Hu, R.J., Wu, J.Z., Li, G.X., Zhu, L.H., Ma, F., 2009. Characteristics of sediment transport in the Zhoushan Archipelago sea area. Acta Oceanol. Sin. 28 (5), 116–127. https://doi.org/10.3969/j.issn.0253-505X.2009.05.014.

Jiang, Z.P., Huang, J.C., Dai, M.H., Kao, S.J., Hydes, D.J., Chou, W.C., Jan, S., 2011. Short-term dynamics of oxygen and carbon in productive nearshore shallow seawater systems off Taiwan: observations and modeling. Limnol. Oceanogr. 56 (5), 1832–1849. https://doi.org/10.4319/lo.2011.56.5.1832.

Laruelle, G.G., Landschützer, P., Gruber, N., Tison, J.L., Delille, B., Regnier, P., 2017. Global high-resolution monthly pCO_2 climatology for the coastal ocean derived from neural network interpolation. Biogeosciences. 14, 4545–4561. https://doi.org/10.5194/bg-14-4545-2017.

Lefèvre, N., Guillot, A., Beaumont, L., Danguy, T., 2008. Variability of fCO_2 in the Eastern Tropical Atlantic from a moored buoy. J. Geophys. Res. 113 (C1), C01015. https://doi.org/10.1029/2007JC004146.

Li, D., Chen, J., Ni, X., Wang, K., Zeng, D., Wang, B., Jin, H., Huang, D., Cai, W.J., 2018. Effects of biological production and vertical mixing on sea surface pCO_2 variations in the Changjiang River plume during early autumn: a buoy-based time series study. J. Geophys. Res.-Oceans 123. https://doi.org/10.1029/2017JC013740.

Lu, Z.M., Gan, J.P., Dai, M.H., 2011. Modeling seasonal and diurnal pCO_2 variations in the northern South China Sea. J. Mar. Syst. 92 (1), 30–41. https://doi.org/10.1016/j.jmarsys.2011.10.003.

Mao, H.L., Gan, Z.J., Lan, S.F., 1963. A preliminary analysis of the Yangtze diluted water and its mixing process (in Chinese with English abstract). Oceanologia et Limnologia Sinica. 5, 183–206.

Middelburg, J.J., Herman, P.M.J., 2007. Organic matter processing in tidal estuaries. Mar. Chem. 106 (1), 127–147. https://doi.org/10.1016/j.marchem.2006.02.007.

Millero, F.J., Graham, T.B., Huang, F., Bustos-Serrano, H., Pierrot, D., 2006. Dissociation constants of carbonic acid in seawater as a function of salinity and temperature. Mar. Chem. 100, 80–94. https://doi.org/10.1016/j.marchem.2005.12.001.

Nemoto, K., Midorikawa, T., Wada, A., Ogawa, K., Takatani, S., Kimoto, H., Ishii, M., Inoue, H.Y., 2009. Continuous observations of atmospheric and oceanic CO_2 using a moored buoy in the East China Sea: variations during the passage of typhoons. Deep-Sea Res. Part II-Top. Stud. Oceanogr. 56 (8–10), 542–553. https://doi.org/10.1016/j.dsr2.2008.12.015.

Ni, Y.Q., Ge, Z.Q., Zhu, J.Z., 2003. Study on characteristic of hydrodynamics in Hangzhou Bay. in Chinese. J. Hydrodyn. 18 (4), 439–445. https://doi.org/10.16076/j.cnki.cjhd.2003.04.009.

Ning, X., Vaulot, D., Liu, Z., Liu, Z., 1988. Standing stock and production of phytoplankton in the estuary of the Changjiang (Yangtze River) and the adjacent East China Sea. Mar. Ecol.-Prog. Ser. 49, 141–150. https://doi.org/10.3321/j.issn:1000-0933.2008.11.065.

Pierrot, D., Neill, C., Sullivan, K., Castle, R., Wanninkhof, R., Lüger, H., Johannessen, T., Olsen, A., Feely, R.A., Cosca, C.E., 2009. Recommendations for autonomous underway pCO_2 measuring systems and data-reduction routines. Deep-Sea Res. Part II-Top. Stud. Oceanogr. 56 (8–10), 0–522. https://doi.org/10.1016/j.dsr2.2008.12.005.

Pu, J.J., Xu, H.H., Kang, L.L., Ma, Q.L., 2011. Characteristics of atmospheric CO_2 concentration and variation of carbon source & sink at Lin'an regional background station. in Chinese with English abstract. Environ. Sci. 32 (8), 2221–2225. https://doi.org/10.13227/j.hjkx.2011.08.036.

Reimer, J.J., Cai, W.J., Xue, L., Vargas, R., Noakes, S., Hu, X., Signorini, S.R., Mathis, J.T., Feely, R.A., Sutton, A.J., Sabine, C., Musielewicz, S., Chen, B., Wanninkhof, R., 2017. Time series pCO_2 at a coastal mooring: internal consistency, seasonal cycles, and interannual variability. Cont. Shelf Res. 145, 95–108. https://doi.org/10.1016/j.csr.2017.06.022.

Revelle, R., Suess, H.E., 1957. Carbon dioxide exchange between atmosphere and ocean and the question of an increase of atmospheric CO_2 during the past decades. Tellus 9 (1), 18–27. https://doi.org/10.3402/tellusa.v9i1.9075.

Schiettecatte, L.S., Thomas, H., Bozec, Y., Borges, A.V., 2007. High temporal coverage of carbon dioxide measurements in the Southern Bight of the North Sea. Mar. Chem. 106 (1–2), 161–173. https://doi.org/10.1016/j.marchem.2007.01.001.

Schlitzer, R., 2013. Ocean Data View. http://odv.awi.de/.

Sutton, A.J., Sabine, C.L., Maennerjones, S., Lawrenceslavas, N., Meinig, C., Feely, R.A., Mathis, J.T., Musielewicz, S., Bott, R., McLain, P.D., Fought, H.J., Kozyr, A., 2014. A high-frequency atmospheric and seawater pCO_2 data set from 14 open-ocean sites using a moored autonomous system. Earth Syst. Sci. Data. 6, 353–366. https://doi.org/10.5194/essd-6-353-2014.

Sweeney, C., Gloor, E., Jacobson, A.R., Key, R.M., McKinley, G., Sarmiento, J.L., Wanninkhof, R., 2007. Constraining global air-sea gas exchange for CO_2 withrecent bomb ^{14}C measurements. Glob. Biogeochem. Cycles 21, GB2015. https://doi.org/10.1029/2006GB002784.

Takahashi, T., Olafsson, J., Goddard, J., Chipman, D.W., Sutherland, S.C., 1993. Seasonal variation of CO_2 and nutrients in the high-latitude surface oceans: A comparative study. Glob. Biogeochem. Cycles 7, 843–878. https://doi.org/10.1029/93GB02263.

Takahashi, T., Sutherland, S.C., Sweeney, C., Poisson, A., Metzl, N., Tilbrook, B., Bates, N., Wanninkhof, R., Feely, R.A., Sabine, C., Olafsson, J., Nojiri, Y., 2002. Global sea-air CO_2 flux based on climatological surface ocean pCO_2, and seasonal biological and temperature effects. Deep-Sea Res. Part II-Top. Stud. Oceanogr. 49, 1601–1622. https://doi.org/10.1016/S0967-0645(02)00003-6.

Tseng, C.M., Shen, P.Y., Liu, K.K., 2014. Synthesis of observed air-sea CO_2 exchange fluxes in the river-dominated East China Sea and improved estimates of annual and seasonal net mean fluxes. Biogeosciences. 11, 3855–3870. https://doi.org/10.5194/bg-11-3855-2014.

Turk, D., Malačič, V., DeGrandpre, M.D., McGillis, W.R., 2010. Carbon dioxide variability and air-sea fluxes in the northern Adriatic Sea. J. Geophys. Res. 115, C10043. https://doi.org/10.1029/2009JC006034.

Wang, L.C., 1990. China-U.S. Joint Muddy Coast Research, Part 1, a Review of hydrological and sedimentary processes in Hangzhou Bay, China.

Wang, J.H., Wu, J.Y., 2009. Occurrence and potential risks of harmful algal blooms in the East China Sea. Sci. Total Environ. 407 (13), 4012–4021. https://doi.org/10.1016/j.scitotenv.2009.02.040.

Wanninkhof, R., 1992. Relationship between wind-speed and gas-exchange over the ocean. J. Geophys. Res. 97 (C5), 7373–7382. https://doi.org/10.1029/92JC00188.

Weiss, R.F., 1974. Carbon dioxide in water and seawater: the solubility of a non-ideal gas. Mar. Chem. 2, 203–215. https://doi.org/10.1016/0304-4203(74)90015-2.

Weiss, R.F., Price, R.A., 1980. Nitrous oxide solubility in water and seawater. Mar. Chem. 8, 347–359. https://doi.org/10.1016/0304-4203(80)90024-9.

Wu, H., Zhu, J.R., Shen, J., Wang, H., 2011. Tidal modulation on the Changjiang River plume in summer. J. Geophys. Res. 116 (C8), C08017. https://doi.org/10.1029/2011JC007209.

Xie, D.F., Wang, Z.B., Gao, S., DeVriend, H.J., 2009. Modeling the tidal channel morphodynamics in a macro-tidal embayment, Hangzhou Bay, China. Cont. Shelf Res. 29 (15), 1757–1767. https://doi.org/10.1016/j.csr.2009.03.009.

Xue, L., Cai, W.J., Hu, X., Sabine, C., Jones, S., Sutton, A.J., Jiang, L.Q., Reimer, J.J., 2016. Sea surface carbon dioxide at the Georgia time series site (2006-2007): air-sea flux and controlling processes. Prog. Oceanogr. 140, 14–26. https://doi.org/10.1016/j.pocean.2015.09.008.

Yates, K.K., Dufore, C., Smiley, N., Jackson, C., Halley, R.B., 2007. Diurnal variation of oxygen and carbonate system parameters in Tampa Bay and Florida Bay. Mar. Chem. 104 (1–2), 110–124. https://doi.org/10.1016/j.marchem.2006.12.008.

Yu, P., Zhang, H., Zheng, M., Pan, J., Bai, Y., 2013. The partial pressure of carbon dioxide and air-sea fluxes in the Changjiang river estuary and adjacent Hangzhou Bay. Acta Oceanol. Sin. 32 (6), 13–17. https://doi.org/10.1007/s13131-013-0320-6.

Zhai, W., Dai, M., 2009. On the seasonal variation of air-sea CO_2 fluxes in the outer Changjiang (Yangtze River) Estuary, East China Sea. Mar. Chem. 117 (1–4), 2–10. https://doi.org/10.1016/j.marchem.2009.02.008.

Zhai, W.D., Dai, M.H., Cai, W.J., Wang, Y.C., Wang, Z.H., 2005a. High partial pressure of CO_2 and its maintaining mechanism in a subtropical estuary: the Pearl River estuary. China. Mar. Chem. 93 (1), 21–32. https://doi.org/10.1016/j.marchem.2004.07.003.

Zhai, W.D., Dai, M.H., Cai, W.J., Wang, Y.C., Hong, H.S., 2005b. The partial pressure of carbon dioxide and air-sea fluxes in the northern South China Sea in spring, summer and autumn. Mar. Chem. 96 (1–2), 87–97. https://doi.org/10.1016/j.marchem.2004.12.002.

Zhai, W.D., Dai, M.H., Guo, X.H., 2007. Carbonate system and CO_2 degassing fluxes in the inner estuary of Changjiang (Yangtze) River. China. Mar. Chem. 107, 342–356. https://doi.org/10.1016/j.marchem.2007.02.011.

Zhao, D.Z., Zhao, L., Zhang, F.S., Zhang, X.Y., 2004. Temporal occurrence and spatial distribution of red tide events in China's coastal waters. Hum. Ecol. Risk. Assess. 10 (5), 945–957. https://doi.org/10.1080/10807030490889030.

Zhou, W., Yin, K., Long, A., Huang, H., Huang, L., Zhu, D., 2012. Spatial-temporal variability of total and size-fractionated phytoplankton biomass in the Yangtze River Estuary and adjacent East China Sea coastal waters, China. Aquat. Ecosyst. Health Manag. 15 (2), 200–209. https://doi.org/10.1080/14634988.2012.688727.